PCCP

Accepted Manuscript

This is an *Accepted Manuscript*, which has been through the Royal Society of Chemistry peer review process and has been accepted for publication.

Accepted Manuscripts are published online shortly after acceptance, before technical editing, formatting and proof reading. Using this free service, authors can make their results available to the community, in citable form, before we publish the edited article. We will replace this *Accepted Manuscript* with the edited and formatted *Advance Article* as soon as it is available.

You can find more information about *Accepted Manuscripts* in the Information for Authors.

Please note that technical editing may introduce minor changes to the text and/or graphics, which may alter content. The journal's standard Terms & Conditions and the Ethical guidelines still apply. In no event shall the Royal Society of Chemistry be held responsible for any errors or omissions in this *Accepted Manuscript* or any consequences arising from the use of any information it contains.

ROYAL SOCIETY OF CHEMISTRY

www.rsc.org/pccp

Direct CO oxidation by lattice oxygen on SnO_2(110) surface: a DFT study

Zhansheng Lu [a], Dongwei Ma [b] , Lin Yang [c], Xiaobing Wang [c], Guoliang Xu [a], and Zongxian Yang [a*]

[a] *College of Physics and Electronic Engineering, Henan Normal University, Xinxiang, 453007, China.*

[b] *School of Physics, Anyang Normal University, Anyang 455000, China.*

[c] *School of Chemistry and Chemical Engineering, Henan Normal University, Xinxiang 453007, China.*

ABSTRACT

As a noble-metal-free catalyst for CO oxidation, SnO_2 is sparked worldwide interest owing to its highly reactive lattice oxygen atoms and low cost. The current density functional theory (DFT) results demonstrate the process of CO oxidation by lattice oxygen on the SnO_2(110) surface and the recovery of the reduced surface by O_2. It is found that CO can be easily oxidized on the SnO_2(110) surface following the Mars−van Krevelen Mechanism. The adsorbed oxygen turns into various oxygen species with transferring electron(s) to the chemisorbed oxygen, which is only found on the partially reduced SnO_{2-x} surface, but not on the perfect SnO_2(110) surface: $O_2(gas) \leftrightarrow O_2(ad) \leftrightarrow O_2^{-}(ad) \leftrightarrow O_2^{2-}(ad) \leftrightarrow O^{2-}(lattice) + O^{-}(ad)$. The calculated stretching frequencies would help to distinguish the various adsorbed species observed in experiment and of course help in the assignment of vibrational modes in the experimental spectra.

* Author to whom correspondence should be addressed.

Electronic mail: yzx@henannu.edu.cn

1 Introduction

The oxidation of CO on heterogeneous catalysts could provide one of the most promising ways for solving current urgent environmental pollution issues, because of its wide applications in automotive exhaust treatment, indoor air cleaning, and breathing apparatus[1-3]. Given the low catalytic activities and poor stabilities of conventional catalysts and the high cost, low abundance and rapid deactivation of the noble metals catalysts, noble-metal-free catalysts have sparked worldwide interest owing to their low cost, environmental friendliness, and outstanding thermal stability in very recent years[3, 4]. To this end, tetragonal SnO_2 was found to be a good choice, mainly due to its highly reactive lattice oxygen atoms and its low cost, minimal toxicity, abundance, and high melting point[5]. Moreover, due to changes in the electrical conductance in response to environmental gases, SnO_2 is also the most employed metal oxide semiconductor as gas sensors for the detection of a wide variety of toxic, combustible and pollutant gases[5].

The CO oxidation depends mainly on the activity of the SnO_2 surface(s), linking with its ability of reduction and oxygen adsorption (recovery). The (five atomic-layer-thick) SnO_2 thin sheets of the (001) surface have been found to be sufficient for catalytic oxidation of CO and facile O_2 dissociation[3]. However, the SnO_2(001) surface has larger surface energy than that of the (110) surface, which is the most stable low-index SnO_2 surface[4, 6]. Usually, the most stable (110) surface would be the most popular one[4, 7]. To reveal the process of CO oxidation on the SnO_2(110) surface and the O_2 healing of the O vacancy (left by CO oxidation) in atomic and electronic level, both CO and O_2 adsorption on various SnO_2(110) surfaces and transition states calculations were performed. We hope to understand the mechanism of the CO oxidation on SnO_2 and shed light on how to improve its activity and the capability of the gas detection. The focusing points are: a) can the CO be oxidized by the lattice O or the atmosphere gas O_2 activated by SnO_2; b) what is the possible reaction path of the CO oxidation on SnO_2; c) how is the SnO_2 surface recovered.

2 Computational Details

2.1 Computational Method

All of the spin-polarized density functional theory (DFT) calculations are performed by DFT program DMol[3] in Materials Studio (Accelrys, SanDiego, CA), using a DFT semi-core pseudopotential[8] with GGA-PBE functional[9]. Complete linear synchronous transit (LST)/quadratic synchronous transit (QST) calculations are performed to locate transition states (TS). Transition states are identified by the number of imaginary frequencies (NIMG) with NIMG = 1, the vibrational modes, and "TS conformation" implemented in DMol[3]. During geometrical optimization, the basis set cutoff is chosen to be 3.5 Å. The convergence tolerances for the geometry optimization are set to be 10^{-5} Ha for the energy, 0.002 Ha/Å for the forces, and 0.005 Å for the displacement. The electronic self-consistence field (SCF) tolerance is set to 10^{-6} Ha. A Fermi smearing parameter of 0.005 Ha is used in the calculations. The reciprocal space is sampled with a (2 × 2 × 1) k-points grid generated automatically using the Monkhorst–Pack method[10]. More details about the DMol[3] code can be found elsewhere[11,

2.2 Models used

The perfect SnO_2(110) surface, the most stable low-index SnO_2 surface[6], is simulated with the periodic slab model (see Fig. 1) composed of four O(Sn2O2)O trilayers and a vacuum layer of 15 Å introduced on the top of the free surface to separate the films. The bottom two trilayers are fixed in their bulk positions to mimic the bulk. According to our tests, the four-trilayer model is sufficient for reproducing the relaxation of atoms on the outermost layer and for correct estimation of adsorption energies.

The adsorption energies, E_{ad}, which measure the stability of the adsorption configurations, are defined as: $E_{ad} = E_{adsorbate} + E_{support} - E_{adsorbate/support}$, where $E_{adsorbate}$, $E_{support}$ and $E_{adsorbate/support}$ are the total energies of the free adsorbate, the corresponding support and the support with the adsorbate, respectively. With this definition, a positive value indicates an exothermic adsorption. For each optimized adsorption system, harmonic C–O or O-O stretching vibrational frequencies, ω(C–O) or ω(O–O), are calculated from a normal coordinate analysis (at the gamma point in the Brillouin zone) involving the CO_x or O_2 group atoms.

The partially reduced SnO_2(110): SnO_2 surfaces are interesting because the presence of two possible oxidation states of tin (+2 and +4), which are combined with the reduced atomic coordination, favourable compositional changes and reconstructions. The analysis of Mulliken atomic charges on the perfect SnO_2(110) surface, which would be taken as the most important references to distinguish the valance state of the various support and adsorbed species, shows that the O ions in the O_{2c} positions (nominally –2 valance state) is negatively charged by 0.71 |e|, denoted as $q(O^{2-})$ hereafter. The Sn ions of the Sn_{6c} (nominally +4 valance state) are positively charged by 1.53 |e|, denoted as $q(Sn^{4+})$ hereafter.

As well-known, the reduced SnO_2(110) surface is formed by the removal of the oxygen atom(s) from the stoichiometric surface. To reveal the properties of the reduced SnO_2 surface, oxygen vacancies (O-vacs) at various locations are created (Fig. 2). It is found that, for one O-vac, the most preferable O-vac is at the O2c position in the first atomic layer of the SnO_2(110) surface. When two O-vacs are created, the most preferable configuration is the one with the two surface O atoms at O2c lost. The calculated vacancy formation energies are 44.1 and 50.1 kcal/mol for the first O-vac and the second O-vac, respectively. Upon the formation of the O-vac at O2c, a charge shrink of about 0.19 |e| (~ 13%) for the two Sn neighbours to the O-vac is found, indicating the formation of Sn^{3+} ions (nominally). With the formation of two O-vacs, the charges of the two Sn neighbours of the O-vacs shrink by ~ 35% (~0.55 |e|), which are related to the $q(Sn^{4+})$, indicating the formation of the 4-fold coordinated Sn^{+2} ions (nominally).

3. Results

For clarity, this section is organized as follows. First, we examine the adsorption properties for all adsorbed species on the various SnO_2 surfaces (SnO_2, SnO_{2-x}). Second, we investigate the most likely reaction steps involved in CO oxidation and the re-fresh of the

SnO_2 surface, through the transition states calculations, so that we can get a general view of the reaction process. The properties of the various configurations are summarized in Fig. 3 and Table I, together with the calculated harmonic frequencies of the C-O and O-O vibrational stretching modes for all the adsorbate species.

3.1 Various configurations and reactions

O_2 on the SnO_2(110) surface, O_2/SnO_2: The adsorption of O_2 on the stoichiometric SnO_2(110) surface is not favourable and only rather weak interaction is found.

CO on the SnO_2(110) surface, CO/SnO_2: Three stable product configurations are found for the adsorption of CO on the SnO_2(110) surface (Fig. 3), "physisorption", "CO_3^{2-}", and "CO_2", and the corresponding properties are presented in Table I. The physisorption has a rather small E_{ad}, while the bigger E_{ad} values are found for the CO_3^{2-} and CO_2 species (cf. Table I). The physisorption of the CO induces negligible modifications in both the adsorbate and surface geometries, while rather strong modifications are found for the cases of the CO_3^{2-} and CO_2 species. Upon the CO_3^{2-}(CO_2) species formation, two of the Sn^{4+} ions are reduced to Sn^{3+}, and two (one) surface O ions are pulled outward from the surface, resulting in the formation of two (one) new C-O bonds, which is confirmed by the corresponding charge density (Fig. 3a) and by the analysis of Mulliken atomic charges to the formed species (cf. Table I).

Stage-1 in Fig. 4 presents the conversion process of the (1st) CO on the perfect SnO_2 surface (the process of CO oxidation on the perfect SnO_2 surface). The reaction starts by the adsorption of CO on a surface lattice tin atom, as the "physisorption" configuration. The following step is the diffusion of the adsorbed CO, which reacts with a couple of lattice oxygen atoms (O2c), via a reaction barrier of 13.2 kcal/mol to form the CO_3^{2-} species. The biggest reaction barrier (15.8 kcal/mol) is found for the conversion of the CO_3^{2-} into the CO_2 species. For the rather weak interaction with the SnO_{2-x} support (small E_{ad}, 2.6 kcal/mol), the CO_2 species would spontaneously release as the free CO_2 at room temperature. The process and the conversion barriers are comparable to the recent reported results on CO oxidation on the SnO_2(101) surface[14].

O_2 on the SnO_{2-x}(110), O_2/SnO_{2-x}: Upon the formation of the CO_2 (as mentioned above), one surface O-vac will be left on the SnO_2(110) surface, named as SnO_{2-x}. When an O_2 adsorbs on the SnO_{2-x}, three stable species, namely "O_2-stand", "O_2-lie" and "O_2-cleavage", are presented in Fig. 3b, with the corresponding properties presented in Table I. Strong interaction is found for all of three configurations, indicating the formation of the chemical bonding (confirmed by the charge density shown in Fig. 3b). The O_2 species in the "O_2-stand" and "O_2-lie" configurations are negatively charged by 0.38 |e| [about half of the $q(O^{2-})$] and 0.56 |e| [close to $q(O^{2-})$], respectively and their O-O bonds are 1.33 Å and 1.43 Å (rather close to the previously reported values of 1.347 and 1.435 Å, respectively[15]). Together with the vibration analysis (presented below), the two species are confirmed as O_2^- and O_2^{2-}, respectively. In the "O_2-cleavage" configuration, the cleavage of the O_2 results in an O atom, which heals the O-vac and is negatively charged by 0.65 |e| [rather close to $q(O^{2-})$], and another dissociated O anchors on the atop of Sn with a Sn-O bond and is negatively charged

by 0.38 |e| [about half of the $q(O^{2-})$], indicating the formation of the O^- species. The O^- species is believed to be more reactive than O_2^{2-} [7]. Moreover, the reduced Sn^{3+} ions are re-oxidized to Sn^{4+} accompanying the healing of the O-vac by O_2. All in all, the current results are in line with the previous theoretical report on the formation of the O_2^- and O^- species on the vacancy site of the reduced SnO_2 surface[15].

Stage-2 and *Stage-3* (Fig. 4) present the diagram of O_2 adsorption and conversion on the SnO_{2-x} support. The free O_2 firstly anchors at the O-vac position as an O_2^- (superoxide) in the "O_2-stand" configuration with negligible energy barrier. Subsequently, the conversion of O_2^- into O_2^{2-} species (peroxy) happens via the energy barrier of 12.5 kcal/mol, similar to that on the $CeO_2(111)$ surface[16], indicating that superoxide might easily transform into peroxide with elevating temperature. The cleavage of the O-O bond in the O_2^{2-} species results in the healing of the O-vac by an O^{2-} as lattice oxygen with an additional O^- species anchored on the Sn5c. The presence of these reactive oxygen O^- species was evident in the temperature-programmed reduction and the process is in well agreement with the recent reports[7, 17]. Moreover, two possible fates of the adsorbed O_2^- are proposed[17]: 1) it can lose an electron and leaves from the surface as a gaseous O_2 molecule; 2) it can gain an additional electron (becoming a peroxide ion), cleaving to atomic oxygen and occupying the lattice oxygen position as O^{2-} anion. According to our calculation, once the O_2^- formed, it will be (a little) more possible to gain an additional electron and converts into an O_2^{2-}, since the E_{ad} of O_2^- (17 kcal/mol) is bigger (but not too much) than the reaction barrier (12.5 kcal/mol). In *stage-3* (Fig. 4), the O_2-lie cleavages into two isolated O ions, with a barrier of 12.4 kcal/mol, which is in well agreement with the previous theoretical report[15]. Thus, the proposed process for the adsorption and conversion of O_2 [7, 18-20], $O_2(gas) \leftrightarrow O_2(ad) \leftrightarrow O_2^-(ad) \leftrightarrow O_2^{2-}(ad) \leftrightarrow O^{2-}(lattice)+O^-(ad)$, can happen only on the $SnO_{2-x}(110)$ support but not the perfect $SnO_2(110)$ support according to our DFT results.

CO oxidation on O_2/SnO_{2-x} , CO/O_2+SnO_{2-x}: When the (2nd) CO adsorbs on O_2+SnO_{2-x}, two stable configurations (Fig. 3c), "physisorption" and "CO_2" with weak and strong interactions, respectively, are found. Similar to that of the "CO_2" species on the perfect SnO_2 surface, the rather weak interaction is also found between the formed CO_2 and the SnO_2 support with a small E_{ad} of 7.0 kcal/mol (ref to the free CO_2).

There are two possible processes for the 2nd CO oxidation as depicted in *stage-4a* and *stage-4b* (Fig. 5), respectively. *Stage-4a* follows *Stage-2* and is related to the CO direct oxidization by the O_2^{2-}, via a reaction barrier of 18.7 kcal/mol, converting into the weakly adsorbed CO_2 species. Similarly, the formed CO_2 could release to atmosphere spontaneously, due to the rather weak interaction. *Stage-4b* follows *stage-3* (the cleavage of the O_2), the CO would spontaneously be oxidized to CO_2 by the O^- from the cleavage of O_2, in line with the reported high activity of the O^- [7, 20].

CO oxidation on SnO_{2-x} , CO/SnO_{2-x}: To clarify whether the CO could be oxidized on the partially reduced $SnO_{2-x}(110)$ surface (with one O-vac), we study the CO oxidation on SnO_{2-x}. Two configurations, "physisorption" and "CO_2" with rather weak and rather strong adsorption, respectively, are found (see Fig. 3d). As mentioned in *stage-1*, the partially reduced SnO_{2-x} is formed upon the 1st CO oxidized to CO_2, and in *stage-5* (Fig. 6), the 2nd CO could also be

oxidized to the CO_2 on SnO_{2-x} from the physisorption but via the rather big reaction barrier with 37.0 kcal/mol (Fig. 6). Again, the formed CO_2 would release spontaneously, due to the weak interaction between CO_2 and SnO_{2-x}-two-O-vac (2.6 kcal/mol, E_{ad} ref to gas CO_2).

O_2 on SnO_{2-x} with two O-vac, O_2/SnO_{2-x}-two-vac: Upon the (2nd) CO_2 formation, two surface O-vac's are left on the SnO_2 surface. Three configurations, "physisorption", "O_2-lie", and "O_2-cleavge (corresponding to the perfect SnO_2 surface)", are found for the O_2 adsorbed on SnO_{2-x}-two-vac (presented in Fig. 3e). The analysis of the Mulliken atomic charges shows that the O_2 species in "O_2-lie" configurations is negatively charged by 0.59 |e|, rather close to the $q(O^{2-})$ ions (0.71 |e|) in the first atomic layer of the perfect $SnO_2(110)$ surface, indicating the O_2^{2-} formation. The two O adatoms from the "O_2-cleavge" configurations heal the two surface O-vacs, resulting the recovery of the reduced SnO_2 surface, i.e. the formation of the perfect SnO_2 surface.

According to the *stage-6* in Fig. 6, there are three steps for the recovery of SnO_{2-x}-two-O-vac support by gas O_2: the physisorption of O_2 (step 1)→ the conversion of the physorbed O_2 into the O_2^{2-} ("O_2-lie") via a reaction barrier of 15.1 kcal/mol (step 2) → the cleavage of the O_2^{2-} (via the reaction barrier of 30.4 kcal/mol) and the recovery of the SnO_2 support.

3.2 Reaction mechanism

According to the discussions above, several possible paths for the CO oxidation on the SnO_2 surface are proposed. The energy barriers (presented in the brackets with the biggest reaction barriers in bold face) of the rate-limit steps would be taken as the judge to distinguish the most possible reaction path:

Path Ia, stage-1 + stage-2 + stage-4a
stage-1: $CO(gas)+SnO_2 \rightarrow CO_2(gas)+SnO_{2-x}$ (15.8 kcal/mol)
stage-2: $SnO_{2-x} + O_2(gas) \rightarrow O_2^{2-}/SnO_{2-x}$, (12.5 kcal/mol)
stage-4a: $CO(gas)+O_2^{2-}/SnO_{2-x} \rightarrow CO_2(gas)+ SnO_2$ (**18.7 kcal/mol**)

Path Ib, stage-1 + stage-2 + stage-3 + stage-4b
stage-1: $CO(gas)+SnO_2 \rightarrow CO_2(gas)+SnO_{2-x}$ (**15.8 kcal/mol**)
stage-2: $SnO_{2-x} + O_2(gas) \rightarrow O_2^{2-}/SnO_{2-x}$, (12.5 kcal/mol)
stage-3: $O_2^{2-}/SnO_{2-x} \rightarrow O^-/SnO_2$, (12.4 kcal/mol)
stage-4b: $O^-/SnO_2 + CO(gas) \rightarrow CO_2(gas) + SnO_2$

Path II, stage-1 + stage-5 + stage-6
stage-1: $CO(gas)+SnO_2 \rightarrow CO_2(gas)+SnO_{2-x}$ (15.8 kcal/mol)
stage-5: $SnO_{2-x} + CO(gas) \rightarrow CO_2(gas) + SnO_{2-x}$-tow-O-vac, (**37.0 kcal/mol**)
stage-6: SnO_{2-x}-tow-O-vac + $O_2(gas) \rightarrow SnO_2$ (30.4 kcal/mol)

The biggest reaction barrier for **Path Ia** is 18.7 kcal/mol for "*stage-4a*", which is quite close to that of the **Path Ib** (15.8 kcal/mol). While the rate-limit step of **Path II** has a much bigger reaction barrier (37.0 kcal/mol). Thus, the **Path Ia** and **Path Ib** are both the most possible reaction paths for the CO oxidation and the recovery of the partially reduced SnO_2 by

O_2 (see Fig. 7). The **Path II** would be only possible in the high temperature due to the big reaction barrier.

3.3 Stretching frequencies of the various species

Vibrational spectra from quantum-mechanical calculations can help to shed light on the nature of the adsorbed species observed in experiment and of course helps in the assignment of vibrational modes in the experimental spectra. The calculated harmonic frequencies of the C-O and O-O vibrational stretching modes for all adsorbate species presented above are given in Table I.

The calculated C–O stretching frequency for the gas phase CO is 2097 cm^{-1}, comparable with the experimental data (2148 cm^{-1})[21] and the previous DFT results (2103 cm^{-1})[22]. The calculated vibrational frequency of the gas O_2 molecule is 1544 cm^{-1}, which is comparable to the experimental value of 1580 cm^{-1}. Three vibrational modes, "Asymmetric Stretch", "Symmetric Stretch" and "Bending Mode" are found for the gas phase CO_2, and their corresponding vibrational frequencies are 2538, 1332, and 670 cm^{-1}, respectively.

The stretching frequencies of the physisorbed CO on the "SnO_2(110)", "O_2+SnO_{2-x}", and "SnO_{2-x}" are found to have blue shifts of about 73 cm^{-1}, 109 cm^{-1} and 77 cm^{-1}, respectively, relative to the gas-phase CO. The three vibrational modes of the two CO_2 formed from the CO on "SnO_2(110)" and "O_2+SnO_{2-x}" are rather close to those of the free CO_2 (except the "Bending mode") with rather small vibrational shift (-1, -17 cm^{-1}, -40 cm^{-1} and 22, -10, -198 cm^{-1} , for the three vibrational modes, respectively), which is in line with the weak interaction between the CO_2 species and the supports.

For the formed CO_3^{2-} on the SnO_2(110) surface, three vibrational modes, "Asymmetric Stretch", "Symmetric Stretch" and "Bending Mode" are found, and their corresponding vibrational frequencies are 1740, 916, and 1021 cm^{-1}, respectively. Moreover, the current results are in well agreement with the previous reported results about the CO_3^{2-} formed on the CeO_2(110) surface (1810 cm^{-1} [23], and 1710 cm^{-1} [22]).

Our calculated vibrational frequency of the O_2^- species formed with O_2 on the defective SnO_2(110) surface is 1203 cm^{-1}, in reasonable agreement with IR spectra (1190 cm^{-1})[13]. On the other hand, the 1045 cm^{-1} band for the vibrations of the O-O bond from IR spectra was also ascribed to the O_2^- species but on the Sn^{2+} [13], while it would be ascribed to the O_2^{2-} species (with the calculated frequencies of 954 cm^{-1} and 1050 cm^{-1}, respectively for O_2^{2-} species on SnO_2 surface with one and two O-vac), due to the low energy barrier of the conversion of O_2^- species into O_2^{2-} species.

4. Conclusions

Summarily, the CO oxidation on the SnO_2(110) surface follows the Mars−van Krevelen Mechanism but not the Langmuir-Hinshelwood Mechanism. The adsorbed oxygen turns into various oxygen species with transferring electron(s) to the chemisorbed oxygen, which is only found on the partially reduced SnO_{2-x} surface but not on the perfect SnO_2(110) surface: $O_2(gas) \leftrightarrow O_2(ad) \leftrightarrow O_2^-(ad) \leftrightarrow O_2^{2-}(ad) \leftrightarrow O^{2-}(lattice) + O^-(ad)$. The calculated stretching

frequencies of the various species would help to distinguish the various adsorbed species observed in experiment and of course helps in the assignment of vibrational modes in the experimental spectra.

Acknowledgements

This work is supported by the National Natural Science Foundation of China (Grant No. 11174070, 11147006, and 11347186), China Postdoctoral Science Foundation funded project (Grant No. 2012M521399) and Postdoctoral Research sponsorship in Henan Province (Grant No. 2011038), Foundation for the Key Young Teachers of Henan Normal University and Start-up Foundation for Doctors of Henan Normal University.

Table I Adsorption energy (E_{ad} in kcal/mol) and bond length ("C-O" or "O-O" in Å) of the various species, Mulliken charges (Δq in |e|) and stretching frequencies (ω in cm^{-1}).

species	Ead	Δq (species)	Δq (Sn)	"C-O" or "O-O"	ω_1	ω_2	ω_3
Partially reduced SnO_2 surface							
1st oxygen-vac	44.1 [a]		0.2				
2nd oxygen-vac	50.1 [a]		0.9				
Gas-phase							
CO		0		1.14	2097		
CO_2		0		1.18	2358	1323	670
O_2		0		1.23	1544		
CO on SnO_2(110)							
physisorption	11.7	0.01	0	1.15	2170		
CO_3^{2-}	26.9	-0.86	0.15,0.08	1.21,1.38,1.37	1740	916	1021
CO_2	33.1 (2.6)[b]	0.01	0.14,0.14	1.17, 1.18	2357	1306	630
O_2 on SnO_{2-x}(110)							
O_2-stand (O_2^-)	17.0	-0.38	1.516	1.325	1203(1190)[c]		
O_2-lie (O_2^{2-})	31.5	-0.56	1.541	1.427	954		
O_2-cleavge (O^{2-}, O^-)	20.3	-1.03			610		
CO on "O_2+SnO_{2-x}(110)"							
physisorption	4.7	0.02		1.14	2206	1127	
CO_2	96.7 (7.0)[b]	0.01			2384	1313	472
CO on SnO_{2-x}(110)							

physisorption	4.8	0.04			2174		
CO_2	30.3 (2.6)[b]	0.02			2369	1324	
O_2 on SnO_{2-x}(110)							
physisorption	6.3	0.003			1590		
O_2-lie	26.2	-0.586			1050		
O_2-cleavge (perfect SnO_2)	93.5	-1.42					

[a] The oxygen vacancy formation energy;

[b] the E_{ad} reference to free CO_2;

[c] IR spectra [13]

Figure Captions

Fig. 1 The SnO_2(110) surface.

Fig. 2 The partially reduced SnO_2(110) surface with one oxygen vacancy (a) and two oxygen vacancies (b), respectively.

Fig. 3 The various adsorption products for CO on SnO_2(110) (a) and O_2 on SnO_{2-x}(110) (b), and the corresponding charge density. CO and O_2 co-adsorption on SnO_{2-x}(110) (c), CO on SnO_{2-x}(110) (d) and O_2 on SnO_{2-x}(110) with two O-vacs (e).

Fig. 4: The conversion process of (1st) CO on perfect SnO_2 surface (stage-1); O_2 adsorption on SnO_{2-x} (stage-2) ; the cleavage of the adsorbed O_2 (stage-3).

Fig. 5 The conversion process of (2nd) CO on O_2+SnO_2 surface before O_2 cleavage

(stage-4a) and after O_2 cleavage (stage-4b).

Fig 6 Various adsorption products for CO on SnO_{2-x}(110) (stage-5), O_2 on SnO_{2-x}-two-vac (stage-6).

Fig. 7 The most possible process for the CO oxidation on SnO_2(110) and the recovery of the SnO_2 by O_2.

References

1. M. Kim, M. Bertram, M. Pollmann, A. v. Oertzen, A. S. Mikhailov, H. H. Rotermund and G. Ertl, *Science*, 2001, **292**, 1357.
2. I. X. Green, W. Tang, M. Neurock and J. T. Yates, *Science*, 2011, **333**, 736.
3. Y. Sun, F. Lei, S. Gao, B. Pan, J. Zhou and Y. Xie, *Angew. Chem. Int. Edit.*, 2013, **52**, 10569.
4. X. Xu, R. Zhang, X. Zeng, X. Han, Y. Li, Y. Liu and X. Wang, *ChemCatChem*, 2013, **5**, 2025.
5. M. Batzill and U. Diebold, *Prog. Surf. Sci.*, 2005, **79**, 47.
6. J. Oviedo and M. J. Gillan, *Surf. Sci.*, 2000, **463**, 93.
7. I. Kocemba and J. M. Rynkowski, *Catal. Today*, 2011, **169**, 192.
8. B. Delley, *Phys. Rev. B*, 2002, **66**, 155125.
9. J. P. Perdew, K. Burke and M. Ernzerhof, *Phys. Rev. Lett.*, 1996, **77**, 3865.
10. H. J. Monkhorst and J. D. Pack, *Phys. Rev. B*, 1976, **13**, 5188.
11. B. Delley, *J. Chem. Phys.*, 2000, **113**, 7756.
12. B. Delley, *J. Chem. Phys.*, 1990, **92**, 508.
13. T. A. Gundrizer and A. A. Davydov, *React. Kinet. Catal. Lett.*, 1975, **3**, 63.
14. J.-M. Ducéré, A. Hemeryck, A. Estève, M. D. Rouhani, G. Landa, P. Ménini, C. Tropis, A. Maisonnat, P. Fau and B. Chaudret, *J. Comput. Chem.*, 2012, **33**, 247.
15. Y. Yamaguchi, Y. Nagasawa, K. Tabata and E. Suzuki, *J. Phys. Chem. A*, 2002, **106**, 411.
16. Y. Zhao, B.-T. Teng, X.-D. Wen, Y. Zhao, Q.-P. Chen, L.-H. Zhao and M.-F. Luo, *J. Phys. Chem. C*, 2012, **116**, 15986.
17. A. Gurlo, *ChemPhysChem*, 2006, **7**, 2041.
18. B. Kamp, R. Merkle, R. Lauck and J. Maier, *J. Solid State Chem.*, 2005, **178**, 3027.
19. S.-C. Chang, *J. Vac. Sci. Technol.*, 1980, **17**, 366.
20. M. A. Mäki-Jaskari, T. T. Rantala and V. V. Golovanov, *Surf. Sci.*, 2005, **577**, 127.
21. P. Reinhardt, M. Causà, C. M. Marian and H. A., *Phys. Rev. B*, 1996, **54**, 14812.
22. M. Nolan, S. C. Parker and G. W. Watson, *Surf. Sci.*, 2006, **600**, 175.
23. Z. Yang, T. K. Woo and K. Hermansson, *Chem. Phys. Lett.*, 2004, **396**, 384.

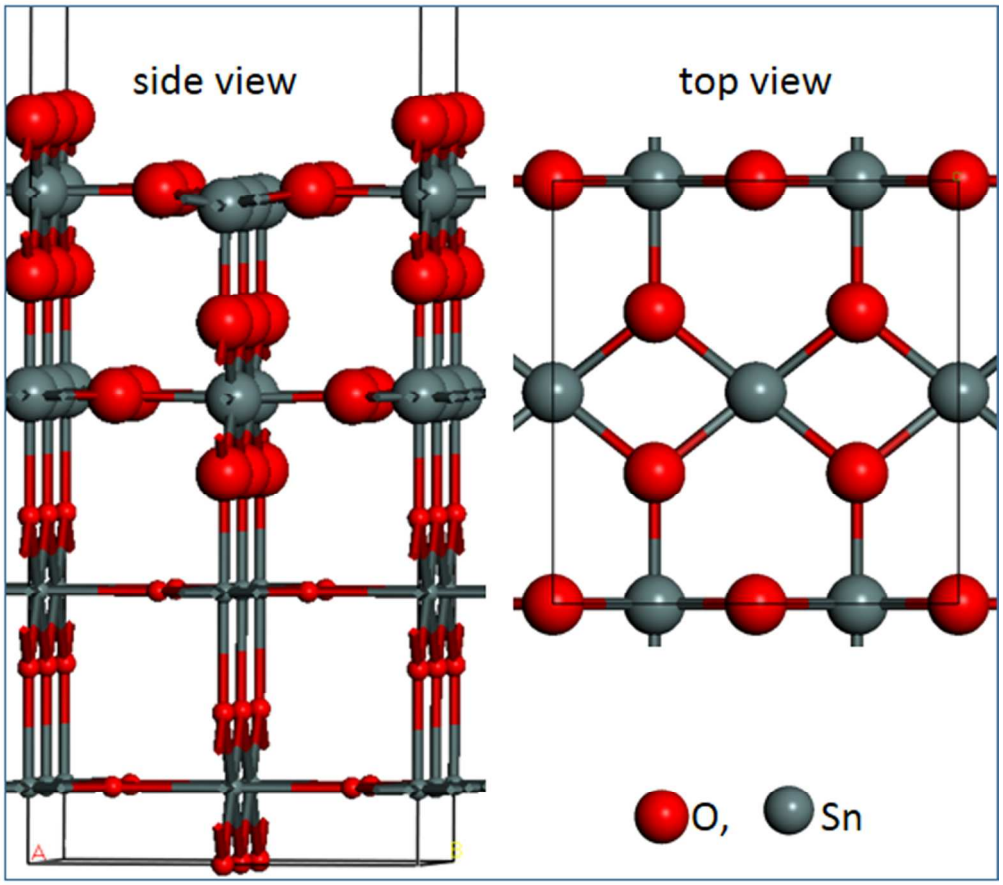

145x129mm (300 x 300 DPI)

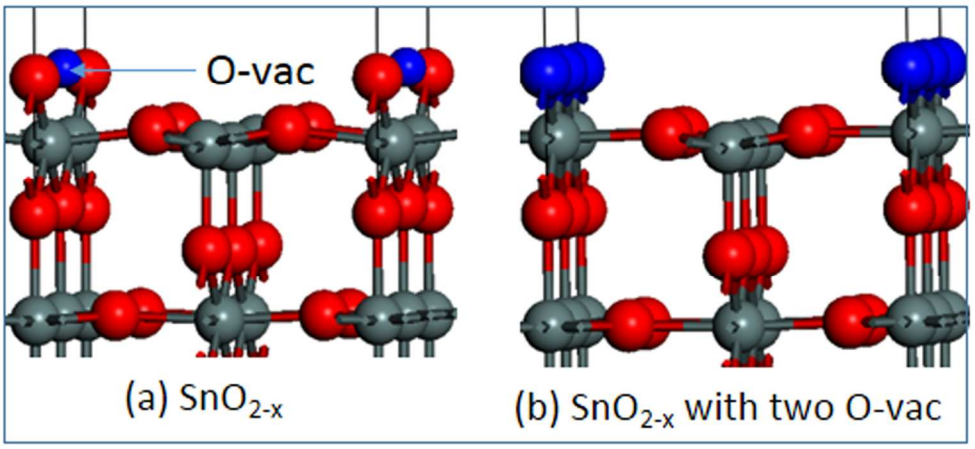

160x77mm (300 x 300 DPI)

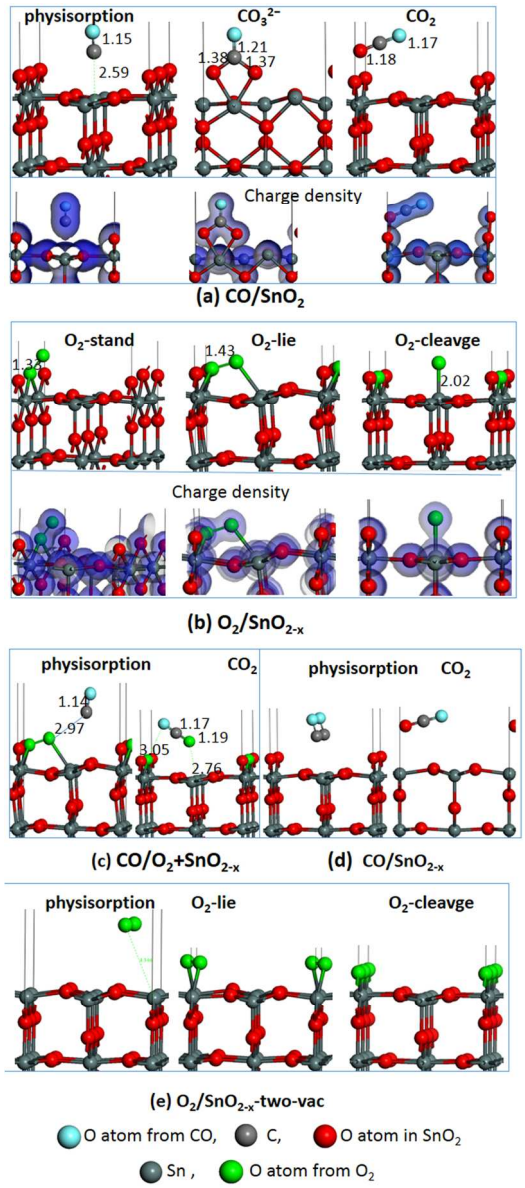

78x180mm (300 x 300 DPI)

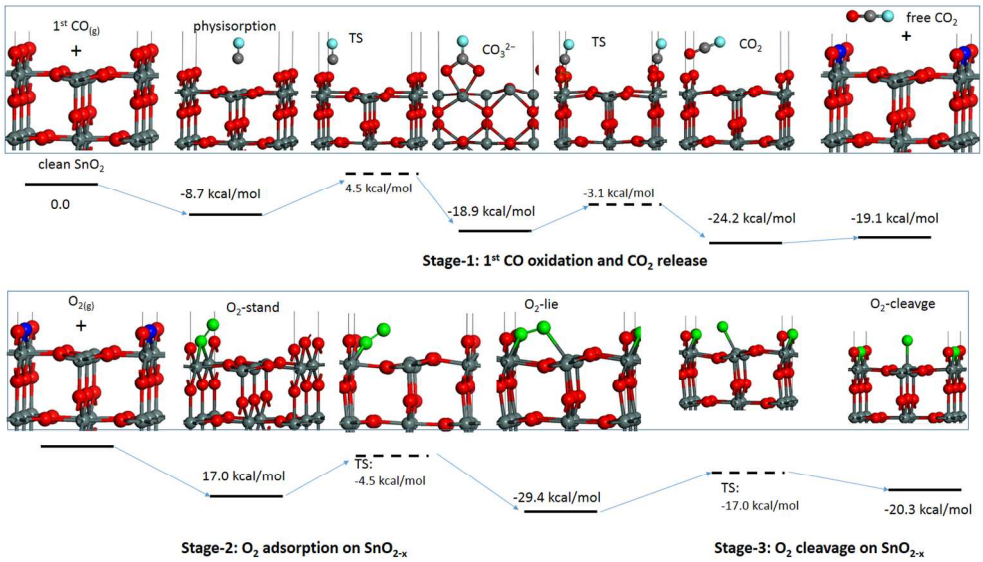

180x102mm (300 x 300 DPI)

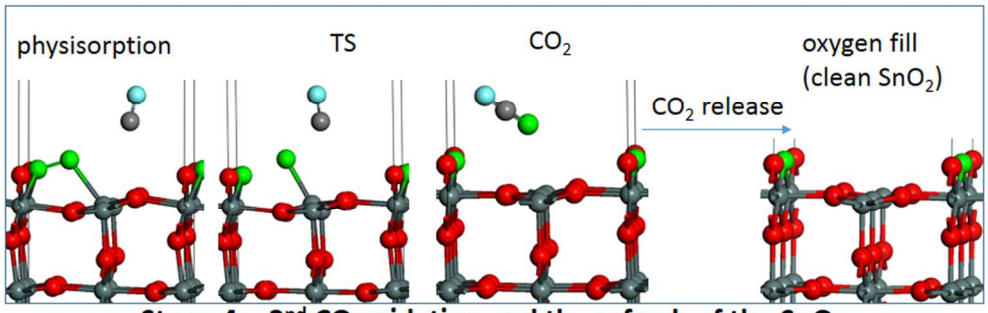

Stage-4a: 2nd CO oxidation and the refresh of the SnO_2

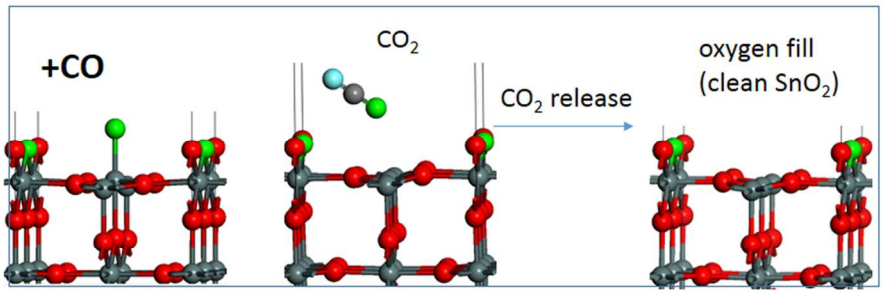

Stage-4b: 2nd CO oxidation and the refresh of the SnO_2

133x99mm (300 x 300 DPI)

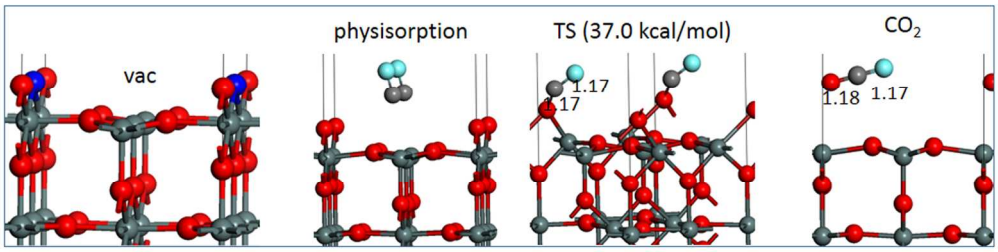

Stage-5: 2nd CO oxidation on SnO_{2-x}

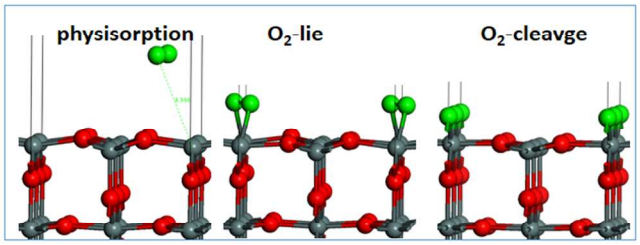

Stage-6: O2 adsorption on SnO2-x-two O-vac and its recovery

180x117mm (300 x 300 DPI)

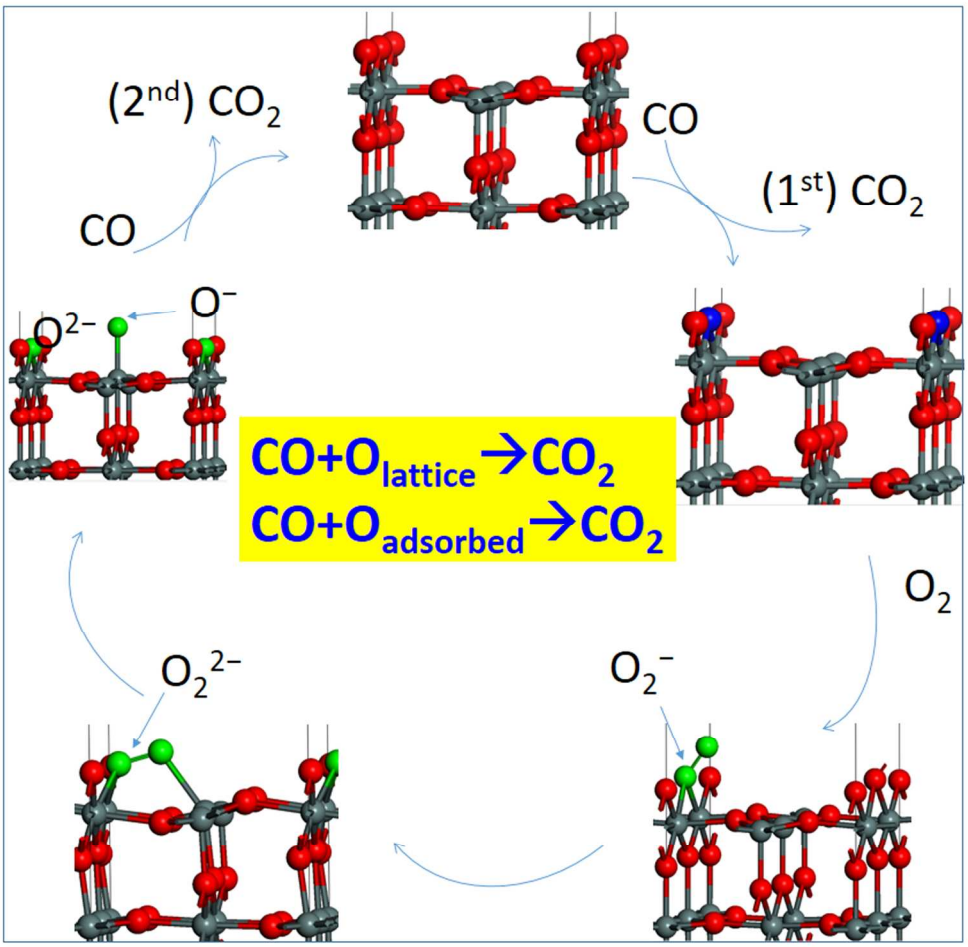

172x164mm (300 x 300 DPI)